Case Study on CFD Simulation and Experiment of New Developed Propeller for Trailing Thai Boat *

J. Noosomton[1], W. Gunnuang[2]

[1,2]IMS, Dept. Marine Engineering, Kasetsart University, Thailand

ABSTRACT

This paper presents to aiming development on a prototype of three-blade propeller for low-speed trailing Thai boat. The uses of the lifting surface designed method were adopted to obtain an optimum shape of the propeller by adjusting the circulation for the maximum lift-to-torque ratio. The blade area was divided into panels of constant radius from hub-to-tip. A three-blades with rake degree angle 18 developed areas 55, defined as New-model which compensation was propeller commonly used of Thai fishermen. The radial distribution of vortex could be determined by a set of constant-strength vortex elements and found that the cavitation had around ship propellers experimentally with new-model appeared to be less than the propeller commonly used of Thai fishermen. This was confirmed by simulation result using CFD. The propeller developed from this proposed design method yielded better performance than the propeller commonly used of local.

Keywords

Rake Angle, Propeller Design, Developed Area, Cavitation.

1 INTRODUCTION

The problem of fishermen in Thailand as the result of that still clings to the old boat and the propellers for used low-speed Trailing-Thai boat has so far based on collective experience obtained from trial of errors. Local casting factories normally developed their design according to field experience of their customers. The development process has not been systematically implemented. Therefore their product performance has been limited and suffered from loss of energy due to low torque to thrust conversion efficiency. Introducing a lifting surface designed method for propeller development work at local level will directly benefit people in local fisheries by reducing cost of fuel consumption.

The current design of low-speed propellers has major issues needing improvement, which are: the blade shape which was not properly developed and optimized for the operating condition and the cavitation that easily occur. These interrelated issues will be focused in this paper. See Fig.(1)

Cavitation is widely known physical phenomena among propeller developers. As the blade rotates, pressure difference occurs across the upper and lower surface of the blade. However, it is desirable to operate the device at maximum possible thrust while keeping the pressure at front side of the propeller above vapor pressure of the fluid. The strategy to avoid cavitation taking place on the surface of the propeller has been a challenging design task to prevent erosion and noise. Cavitation is unsteady in nature created by occurrence of vapor due to pressure drop on the propellers surface. Implosion takes place later on creating periodic pressure fluctuation and vibration of the blade. Recently, computational fluid dynamics (CFD) has played an important role in design process of ship propellers, while a conventional method so-called lifting surface designed method "which an improvement of the lifting line model was developed in the 1980's (Greeley and Kerwin) is still widely used in ship propeller design. By assuming the blade of propeller is a thin sheet upon which the vortices are placed to create the camber line of the blade throughout the spanwise and chord directions. The surface is discretized into small elements containing constant-strength vortex which are determined at certain points between the elements. Their distributions were obtained by coupling with the boundary conditions. The time-independent sources are distributed over the blade by splitting it into small strips at different discretized radial positions.

Design methodology for low-speed propeller in developing world has not been systematically put into record. This paper discusses on the achievement made in using lifting surface designed method for low-speed propellers for trailing-Thai boat driven by small diesel-engine. The blade obtained from this design method will then be analyzed using computational fluid dynamics as well as tested for the cavitation performance in the water tank test facility.

2 DESIGN METHOD

Initially, rake angle, skew angle and developed area were pre-defined. Then, the parameters to be determined were the section thickness distribution, radial distribution of pitch, chord-wise and radial distributions of camber. In order to obtain the new design, the source and vortex distributions representing the blades and their wakes need to be placed on suitable locations to enable the induced velocity field. By adopting linear theory, it is assumed that the perturbation velocities due to the propeller are small

*

Figure 1: Illustrations of tailing Thai boat with 2-blades type which commonly used of Thai fishermen

compared with the inflow velocity. However, the real viscous and turbulent behavior of flow shows the phenomenon of divergence, for instance, in the calculation of the radial loading parameter. The divergence becomes larger when using this method for determination of camber and angle of attack. This could be overcome by the variety of correction procedure adopted for the lifting line method. Figs (2), (3) show the procedure of mentioned design method.

The propeller is considered as a set of blades where "radial lifting lines" are defined starting at hub radius r_h and extends to propeller radius r. A cylindrical coordinate system (z, r, θ) is assumed to be rotating with the propeller, Kerwin (2003). The strength of bound vortices on the blades is the circulation distribution over the blades, $\Gamma(r)$. The lifting lines represent blades of the propeller. The blade is assumed having uniform angular spacing and equal loading. The pitch, camber chord-length etc. of the actual propeller are replaced by a radial distribution of circulation. The lifting lines rotate with angular velocity ω around the z-axis. The shape of the free vortex wake is assumed to be helical. However, under the linear lifting line method, the pitch $\beta(r)$ of the helixes can be determined by the propellers rotation and undisturbed inflow: See equation (1)

Where, $V_a(r)$ is an effective axial inflow and $V_t(r)$ is an effective tangential inflow for each radius over the blades. The shape of the helixes can also be aligned with the induced velocities at the lifting line. For a propeller with optimum radial load distribution, the efficiency for each blade section should be constant and equal to:

$$\beta(r) = \tan^{-1}\left[\frac{V_a(r)}{\omega r + V_t(r)}\right] \tag{1}$$

$$\frac{\tan\beta(r)}{\tan\beta_i(r)} = \text{Conts.} \tag{2}$$

Here, β_i is the hydrodynamic pitch angle and can be given as:

$$\beta(r) = \tan^{-1}\left[\frac{V_a(r) + \bar{u}_a(r)}{\omega r + V_t(r)}\right] \tag{3}$$

$\bar{u}_a(r)$ is the axial induced velocity due to the helical free vortex system. Similarly, the Betz condition can be extended to the case of non-uniform axial inflow, according to condition recommended by Lerbs H.W (2014).

$$\frac{\tan\beta(r)}{\tan\beta_i(r)} = Y\sqrt{1 - w_x(r)} \tag{4}$$

Here, $w_x(r) = 1 - [V_a(r)/V_s]$

When V_s is the speed of a ship and γ is an unknown constant, the forces acting on radius r on the lifting line can be developed from a local application of the Kutta-Joukowski theorem. These forces can then be resolved into components in the axial and tangential directions. Integrated over the radius, and summed over the number of blades to produce the total propeller thrust and torque values. Details about the lifting line theory for propeller can be found in Kerwin (2001).

The continuous distribution of vortices along the lifting line is discredited by vortex lattice elements with constant strength. The element arrangement along the lifting line employs both uniform spacing and cosine spacing. The induced velocity is calculated at control points located at the

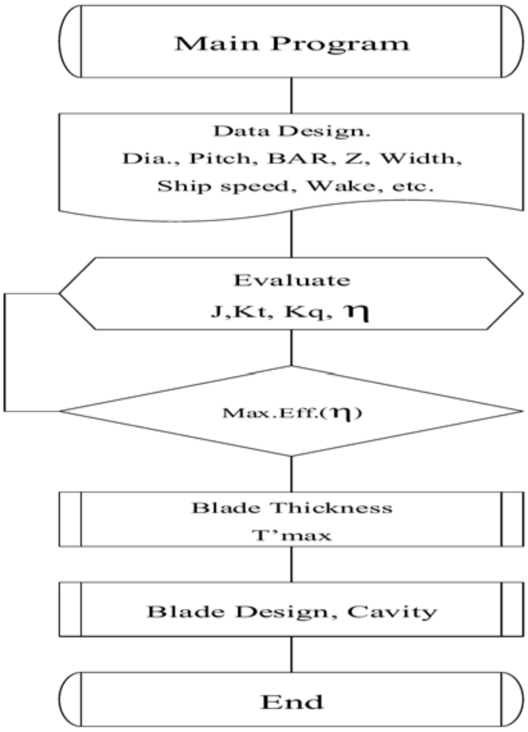

Figure 2: Flow-chart for the determination of an optimal propeller configuration.

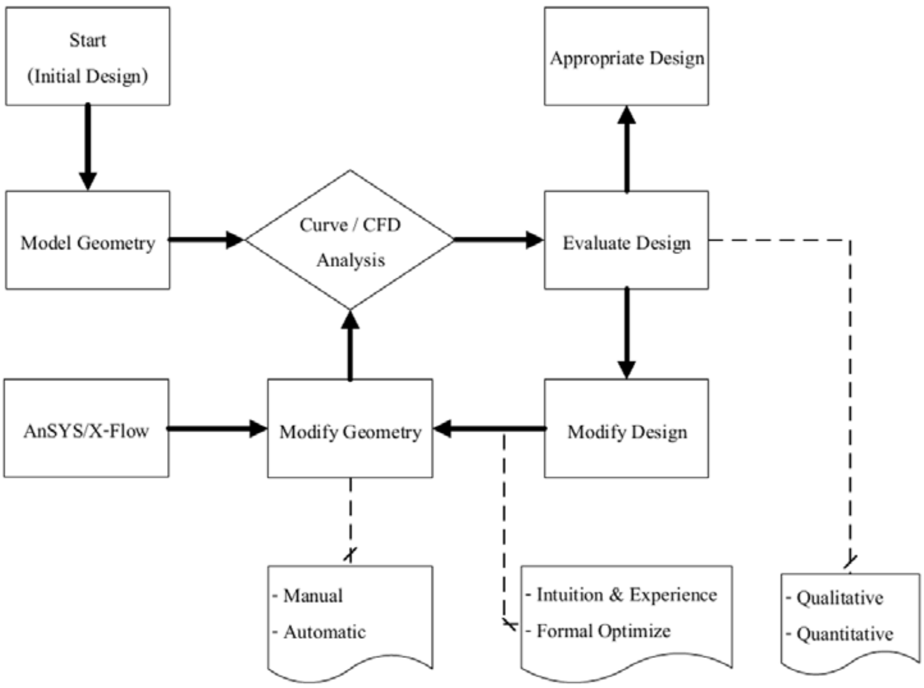

Figure 3: Conceptual design and analysis blade Model

mid-radius of each panel. Thus, the radius of each lifting line is divided into x panels of length Δr and the continuous distribution of circulation over the radius can be replaced by step-like distribution. The value of the circulation in each panel $\Gamma(i)$ is set equal to the value of the continuous distribution at the control points. Since the circulation is piecewise constant, the helical free wake vortex sheet is replaced by a set of concentrated, helical vortex sheds from each panel boundary. The strength of these trailing vortices is equal to the difference in bounded vortex strength across the boundary.

Therefore, it can be considered that the continuous vortex distribution is to be replaced by set of vortex horseshoes. Each of horseshoe line contains the bound vortex filament and the 2-helical trailing vortices. The velocity induced at the lifting line by this system of vortices can be computed using the very efficient formulas given by Kerwin (2001) which are not repeated here. The velocity at a given point is a summation of the velocities from vortex horseshoes.

$$\bar{u}_t\left[r(i)\right] \equiv \bar{u}_t(i) = \sum_{x=1}^{x} \Gamma_{(x)} \bar{u}'_t(i,x) \tag{5}$$

$$\bar{u}_a\left[r(i)\right] \equiv \bar{u}_a(i) = \sum_{x=1}^{x} \Gamma_{(x)} \bar{u}'_a(i,x) \tag{6}$$

Where $\bar{u}_a$ and $\bar{u}_t$ are the axial and tangential components of induced velocity respectively. $\bar{u}'_a$ And $\bar{u}'_t$ are the axial and tangential components of induced velocity at the control point at radius $r(i)$. Integration of the total forces is replaced by the summation over the number of panels. Consider the propeller rotating with constant angular velocity in an axis-symmetric incoming flow field V it same conclusion can be drawn for the simpler case of a wing subjected to a uniform inflow, neglecting the angular velocity term. In the (x_p, y_p, z_p) coordinate system that rotates with the propeller, the total velocity vector V can be written as the sum of the relative undisturbed inflow V_{rel} and the perturbation potential velocity q_{ind}, due to the velocity influence of the propeller itself on the velocity field:

$$V = V_{rel} + q_{ind} \tag{7}$$

Where the relative velocity V_{rel}, in the propeller reference system, can be written as:

$$V_{rel} = V_\infty - \omega \times r \tag{8}$$

With the assumption of an inviscid flow, irrotational flow and incompressible fluid, the perturbation velocity can be written in terms of a scalar function, the perturbation potential, which satisfies the Laplace equation:

$$q_{ind} = \nabla\phi, \quad \nabla^2\phi = 0 \tag{9}$$

By applying Greens second identity for the perturbation potential, the differential equation (9) can be written in integral form with respect to the potential ϕ_p at every point p laying on to the geometry boundaries. The perturbation potential ϕ_i represents the internal perturbation potential, that must be set equal to zero in order to simulate fluid at rest inside the boundaries of all the bodies subject to the external inflow (Blade, hub).

$$\begin{aligned} 2\pi\phi_p = &\int_{S_B+S_{CB}} \left[\phi_q - \phi_{q_i}\right] \frac{\partial}{\partial n_q}\frac{1}{r_{pq}} dS \\ &- \int_{S_B+S_{CB}} \left[\frac{\partial\phi_q}{\partial n_q} - \frac{\partial q_i}{\partial n_q}\right] \frac{1}{r_{pq}} dS \\ &+ \int_{S_w} \Delta\phi_q \frac{\partial}{\partial n_q}\frac{1}{r_{pq}} dS \end{aligned} \tag{10}$$

When subscript q corresponds to the variable point in the integration, n is the unit normal to the boundary surfaces and r_{pq} is the distance between points p and q. equation (10) expresses the potential on the propeller blade as a superposition of the potential induced by a continuous distribution of the sources on the blade and hub surfaces and a continuous distribution of dipoles on the blade, hub and wake surface that can be calculated, directly, via boundary conditions, or indirectly inverting equation (10).

For the solution of equation (10) a certain number of boundary conditions must be applied. Different approaches are possible: a fully linear approach, in which cavity velocities can be considered enough small to allow linearization of boundary conditions or a fully nonlinear one, in which singularities are located on the cavity surface that need to be found iteratively. On the other hand, assumed on the wetted part of the body the kinematic boundary condition holds and allows defining the source strengths in terms of the known inflow velocity relative to the propeller reference system:

$$\frac{\partial\phi_q}{\partial n_q} = -V \cdot n_q \tag{11}$$

At the blade tailing edge the Kutta condition states that the flow must leave with a finite velocity or that the pressure jump at the blade trailing edge must be zero. In a steady problem, the Kutta condition allows to write the dipole intensities, constant along each streamlines, on the wake, first, applying the linear Morino Kutta condition:

$$\Delta\phi_{T.E.} = \phi^U_{T.E.} - \phi^L_{T.E.} + V_{rel} \cdot r_{T.E.} \tag{12}$$

When the subscripts U and L stand for the upper and the lower face of the trailing edge, after the zero pressure jumps can be achieved via an iterative scheme. In fact the pressure difference at trailing edge at each m streamlines is a non linear function of dipole intensities on the blade:

$$\Delta p_m(\phi) = P^U_m(\phi) - P^L_m(\phi) \tag{13}$$

3 RESULTS AND DISCUSSION OF PROPELLER MODEL

The characteristic curves under cavitation conditions can be determined from method given in previous section. The characteristic curves illustrate thrust and torque coefficients as dependent parameters of the advance number obtained from each advance velocity. To obtain the curves, the rotational speed was kept constant and the advance velocity was varied within the operation range of tank test (e.g., in the current tank test, 0 - 3.5 m/s), see Fig.4, Fig.5, Fig.6 and Fig.7. This section also illustrates the test results of newly designed New-model propellers. The main purpose of this performance test was to compare the behavior of occurring bubble at various rotational speeds. The solution at design condition with advance number (J) close to 0.701, as shown in Table(1), has been selected over a wide range of operational conditions between J = 0.1 and J = 1.2

Dimensional analysis used for deriving non-dimensional coefficients in characteristic curves can be found in text book on fundamentals of marine engineering, i.e.; T.P. O'Brien Cgia (1969), Dyson (1924), Jackson (1920). It is therefore not given in this paper. In cavitation analysis, two kinds of curves were derived. One was the characteristic curve at constant cavitation number of 1.386, see Fig.4 and Fig.5. The second was the diagram showing deviation of torque-thrust coefficients and efficiency obtained from experiment on the basis of the given cavitation number. To obtain the result, the static pressure and advance velocity inside the cavitation tunnel test section were lowered gradually in order to sketch the required diagrams. In this paper the discussion on this result has been given in later section, while axial velocity was measured between 0.3 to 3.5 m/s Theoretical thrust and torque coefficients (Kt, Kq) and efficiency (η) of the propeller versus advance coefficients (J_s) is given in Fig.6 and Fig. 7, it is directly proportional to (Kt/J^2, Kq/J^3).

The results of propellers for non-cavitation conditions are essential before proceeding to cavitation conditions for two reasons. *Firstly*, it will be a platform where the numerical method is validated for simulation of the fluid flow around the propeller models. *Secondly*, solving the flow fields in non-cavitating conditions is used as the initial condition for cavitation simulation. The blade was designed up to maximum rotational speed of 1,200 rpm when maximum cavitation was designated to occur. Due to limitation of test tank facility, however, operating condition was carried out between 650 to 850 rpm. These data were used as a design condition for the new-model and therefore used as an operating condition in order to carry out the experimental result.

The design process to increase efficiency of a new-model propeller from width-chord tip propeller in Fig.8 using auto-cad design and macro-excel program by researcher. The wake field is strongly dependent on the ship form and each ship has a unique wake field. In a design stage of the propeller, nominal wake measured in a tank test is used. However, wake field sensitively affects to compute pressure fluctuations on the hull surface. I literature review found that, reproduce an effective wake using a method suggested by Lee et al. (1991).

Fig.9 Shows distance from max thickness to trailing edge and distance from max thickness to leading edge. On the basis of the lifting surface theory, information on circulation distributions on the blade is important. So, there must calculate circulation of the parent propeller and use it to design a new-model propeller giving the same thrust coefficient (K_T) at the same design point to propeller, and It results in discrepancies as both propellers have different pitch and camber distributions. *First*, geometric information such as pitch and camber distributions of new propellers are investigated and fared to give the same thrust to propeller. *Second*, open water performance is calculated and its augmentation is investigated. And also structural strengths and pressure fluctuations are also examined and these are constrained to meet the required conditions. As one increases the area of the propeller blade, cavitation may be decreased but efficiency is consequently decreased (Carlton 2007). So, one may decrease the area of the propeller in a range of allowance of required pressure fluctuations on the hull surface. Using information of series propeller data Chang-Sup Lee (2010), and I can find how much reduction of the expanded area and can increase how much efficiency. For this case, open water efficiencies of propeller are AE/AO = 55 and $\bar{\eta} = 0.69$.

The result of blade design by panel-method and lift-line method yields a set of coordinates of propeller blade as shown in Tables (2) and (3).

The values on the table were taken to construct a blade shape by computer aided design software, see in Fig.(10) and take model was carved into a prototype for aluminum die casting, see in Fig.11 A3-D model shown in Fig.(12) was made for CFD simulation with X-Flow, and ANSYS and compared with result from the laboratory test, specifically on the occurrence of cavity.

4 A. DISCUSSION CAVITATION TEST RESULTS OF NEW-MODEL

The misbelieve among local fishermen regarding the role of cavitation bubbles on performance of the propeller is the major cause of inefficient use of propeller in Thailands local fishery industry. It is necessary to provide strong evidence how generated bubbles could deteriorate the blades mechanical integrity and to see how bubbles could have negative impact to the blade performance. The test results of New-model in non-cavitation state with the rotational speed of 650 rpm are given in Fig.(13), and the results for rotational speed of 750 rpm are given in Fig.(14) Finally, the results for rotational speeds of 850 rpm illustrated in Fig.(15) a summary of experimental test cases selected for comparison in this study.

CFD simulation has played important roles in analysis of flow behavior around the blade. In this study, the geometry and shape of the blade as given in Table (1) was set in the computational domain, while the rotational speed was set at 750 and 850 rpm. A blade with rake angle of 18 degrees was operated at the rotational speed of 650 rpm, as depicted in Fig.(13). When using X-Flow to perform a simulation at 750 rpm in order to recheck the performance of the blade. Certain degree of bubbling flow also occurred at this operating condition, see Fig.(14). It was also found

Table 1: Dimensions and Operating conditions of propellers.

Model Name	New-Model
Diameter, (m)	0.24
Number of blades	3
Effective Rake	18°
Expanded area (Ae/Ao)	55
$(P/D)_{mean}$	0.940
Hub-diameter, (mm.)	40
Ship speed, (Knot)	10
Full-scale propeller, (rpm)	1,200
Propeller rotational speed Test, (rpm)	850
Advance coefficient	0.701
Thrust coefficient	0.181
Open W. eff.	0.691
Cavitation number, $\sigma_{n@0.7R}$	1.386

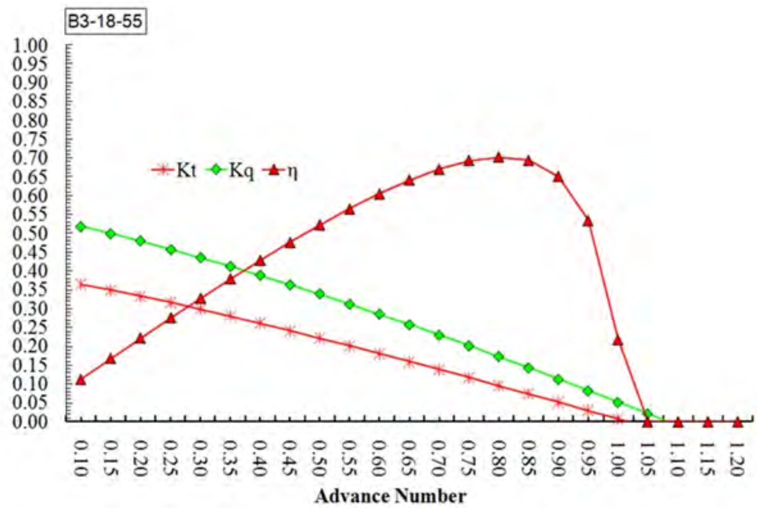

Figure 4: Propellers performance characteristic curves, new-model type 3B-18-55

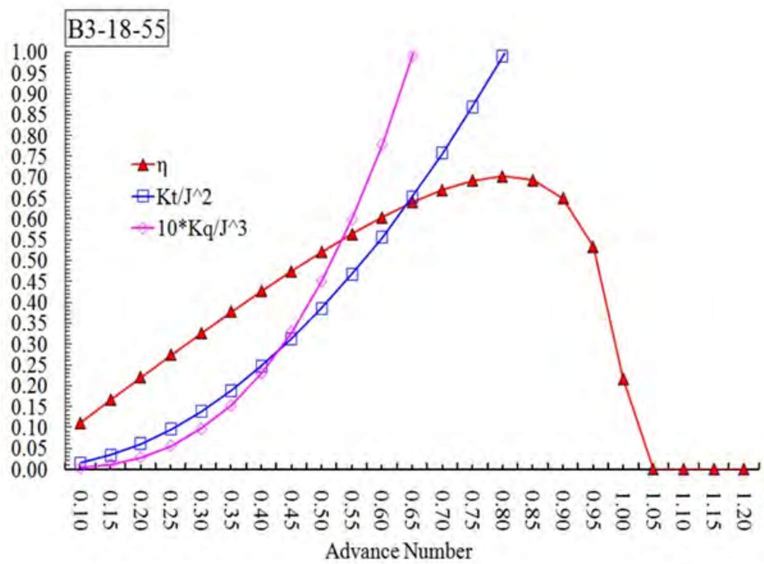

Figure 5: Propellers performance characteristic curves of new-model type 3B-18-55

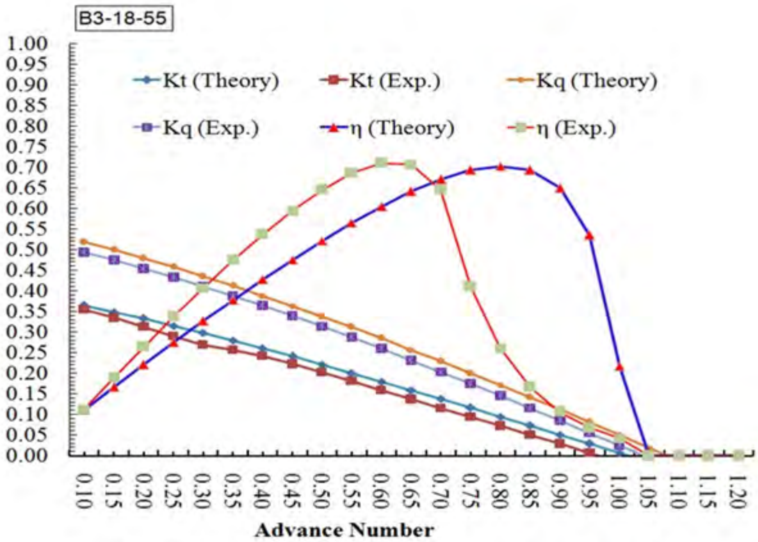

Figure 6: Comparison on the performance curves of Kt, Kq and η, New-model

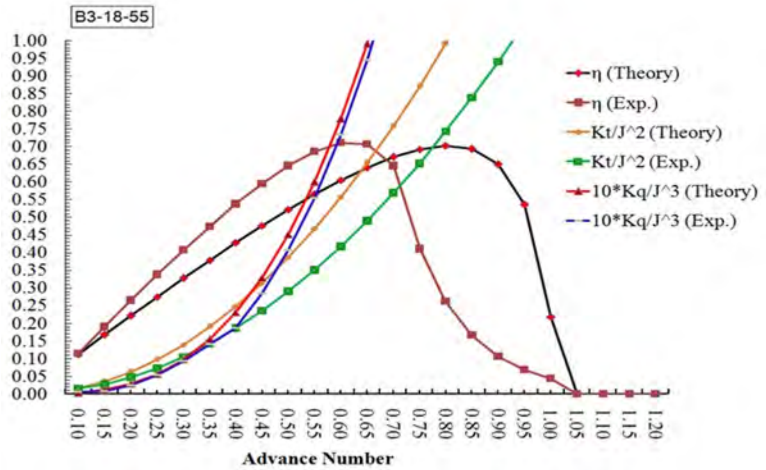

Figure 7: Comparison on the performance curves of inverse Kt, Kq and η, New-model

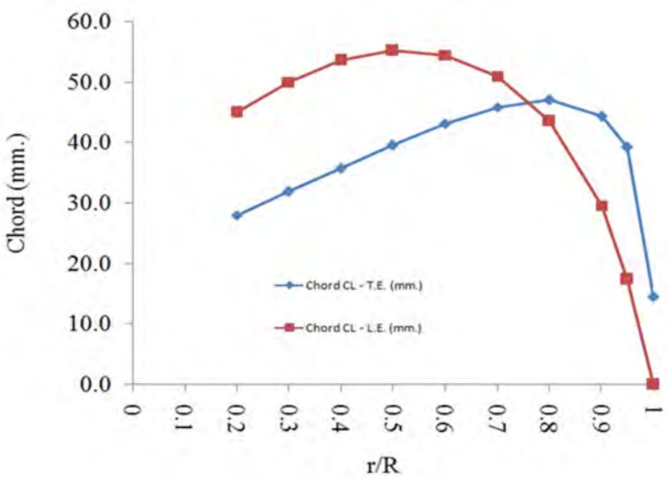

Figure 8: Chord distributions of the width-chord tip blade

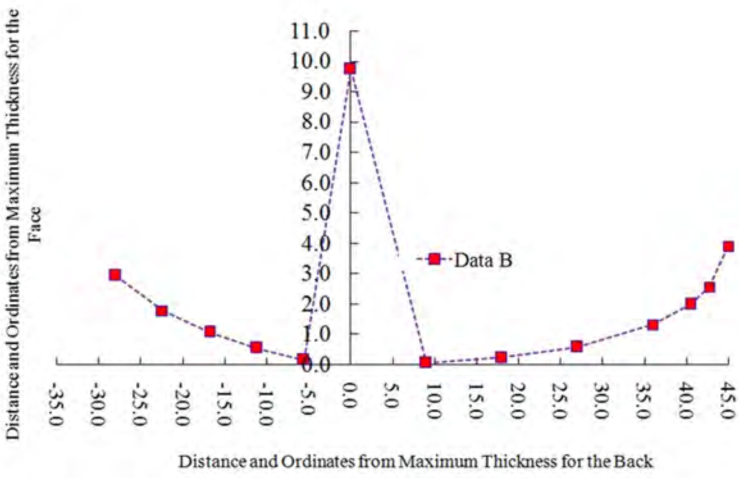

Figure 9: Chord distributions of the wide-chord tip blade

Table 2: Propeller Geometry of Coordinate Thickness New-model; Type 3B-18-55

Backyard of Blade													
r/R	Trailing Edge					T'max	Leading Edge						
	100%	80%	60%	40%	20%		20%	40%	60%	80%	90%	95%	100%
0.95		0.32	0.52	0.63	0.70	0.72	0.70	0.64	0.52	0.32	0.21	0.16	
0.90		0.83	1.29	1.61	1.79	1.85	1.79	1.61	1.29	0.83	0.56	0.41	
0.80		1.22	2.02	2.54	2.88	2.98	2.89	2.54	2.04	1.44	1.03	0.76	
0.70		1.62	2.75	3.48	3.97	4.10	4.01	3.64	3.07	2.34	1.81	1.44	
0.60		2.10	3.51	4.47	5.06	5.23	5.13	4.77	4.15	3.33	2.73	2.27	
0.50		2.76	4.35	5.48	6.17	6.36	6.24	5.88	5.23	4.31	3.61	3.09	
0.40		3.57	5.26	6.48	7.26	7.49	7.35	6.98	6.31	5.27	4.50	3.91	
0.30		4.39	6.17	7.48	8.34	8.62	8.48	8.10	7.39	6.25	5.40	4.73	
0.20		5.20	7.08	8.47	9.25	9.74	9.61	9.21	8.48	7.25	6.27	5.55	
Front of Blade													
r/R	100%	80%	60%	40%	20%	T'max	20%	40%	60%	80%	90%	95%	100%
0.80						2.98							0.22
0.70						4.10					0.20	0.10	0.66
0.60	0.27					5.23				0.04	0.23	0.44	1.28
0.50	0.62	0.11				6.36			0.04	0.27	0.54	0.85	1.93
0.40	1.34	0.46	0.11			7.49		0.02	0.20	0.58	0.94	1.34	2.58
0.30	2.18	1.05	0.50	0.15		8.62		0.11	0.40	0.93	1.43	1.91	3.24
0.20	2.92	1.77	1.06	0.53	0.15	9.74	0.04	0.22	0.57	1.31	1.98	2.55	3.90

Table 3: Propeller Geometry of Coordinate Length New-model Type 3B-18-55

r/R	0.2	0.3	0.4	0.5	0.6	0.7	0.8	0.9	0.95	1
Length: C_L - T.E.	25.45	29.00	32.50	35.97	39.21	41.69	42.80	40.35	35.63	13.20
Length: C_L - L.E.	40.87	45.48	48.73	50.17	49.54	46.35	39.61	26.90	15.82	0.00
Total L.	66.32	74.47	81.23	86.14	88.75	88.03	82.41	67.25	51.44	0.00
T'max to L.E.	23.21	26.07	28.43	30.58	34.52	38.91	39.39	33.62	25.72	0.00
Blade Thickness @ Radius	0.97	0.86	0.75	0.64	0.52	0.41	0.30	0.18	0.07	0.00

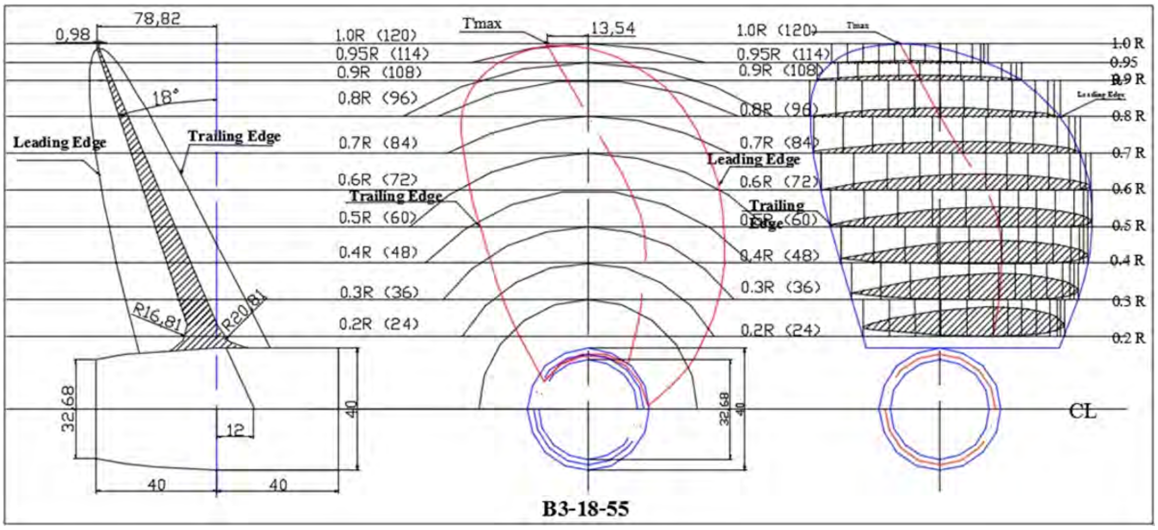

Figure 10: Drawing of propeller design, Type 3 Blades, Rake degree angle 18, Developed area 55

Figure 11: Casting blade of New-model; Type 3B-18-55

that there were a ring of cavitation occurring with certain degree of severity at the rotation speed of 850 rpm as given in Fig.(15). The computation domain 3.3 Million mesh and the contour plots of velocity, static-pressure and cavitation pressure and the predicted on the back sides of the blades are show in Figs.(16), (17), (18) and (19) respective. In addition to the above finding regarding the improved performance of the proposed design from the conventional propeller, the simulation performed as illustrated in Figs.(14), (15), also provided the predictive reliability of the simulation in fully viscous fluid with multi-phase flow as it was in good agreement with the experimental result.

Furthermore, this study on the cavitation pattern of a new propeller in a given onset of flow had confirmed that the performance of the designed geometry is verified and hence the reliability of the propeller design procedure based on viscous flow modeling can be used as a design method for low-speed propeller. Compared to the baseline propeller, the proposed design are characterized as increased in efficiency at high values of the advance coefficient, whereas limited loss of performance are observed at low advance number. These results highlight the importance in development of the present methodology in order to include multiple design points over a wide range of operating conditions, as to ensure an optimized blade design for each particular operating condition.

In addition to laboratory test, activity on field test was carried out at Nakorn Sri-Thammarat province. A numbers of prototypes had been given to local fishermen for free trials with the aim to promote the new propeller design approach to local community. With much improvement in efficiency, it is expected that new propeller will be popular among locals thus enabling significant development in the foundry industry relating to production of low speed propellers. As

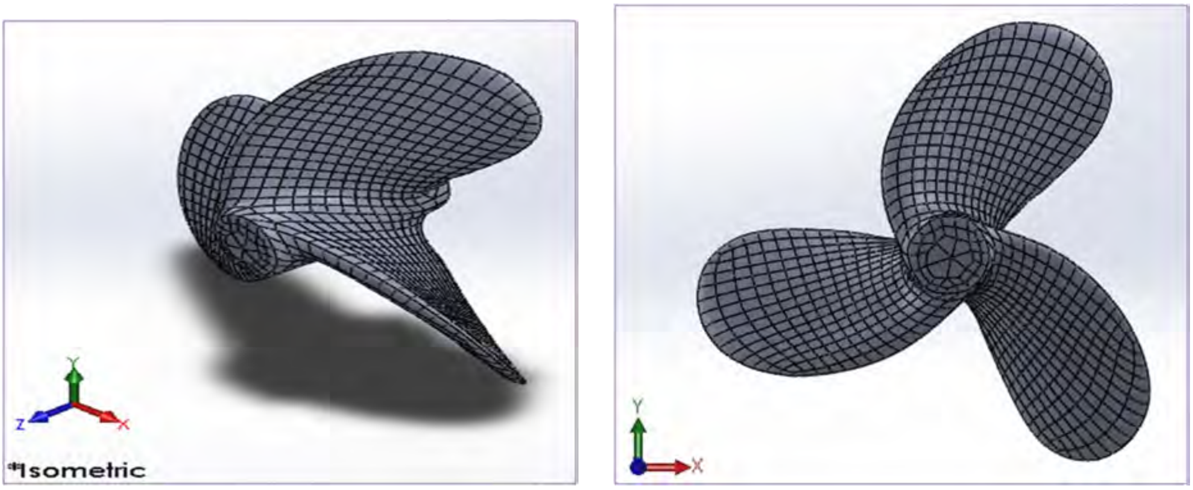

Figure 12: Illustration contours surface of blade New-model; Type 3B-18-55

Figure 13: Illustration of occurrence cavity at rotational speed 650 rpm New-model; Type 3B-18-55

a result, the boat would have better performance. This also results in direct and indirect impact to local community. Firstly, improvement of propeller designs directly result in reduction in fuel consumption, mitigate misunderstanding and misuse that lead to loss of time and opportunity of the locals. Upgrading from 2-blade to 3-blade propellers will reduce a long-term operating cost, since the blade was specifically designed for Trailing Thai boat. Secondly, the dissemination of new design would indirectly contribute to the quality of life of the local fishermen.

Remark: In this limit condition of lab-test, the researchers used a canon camera without stroboscopic flash and laser.

CONCLUSIONS

In this paper, the development on shape of the blade had been proposed for propeller used in low-speed trailing Thai boat. The elucidation bursting phenomenon of tip vortex cavitation in a tank test was carried out with new-model propeller. Their cavitation characteristics had been investigated experimentally at advance speed of 3.5 m/s. The experimental results revealed that new blades showed blade tip cavitation within the operating speed of 650 and 850 rpm while appeared to be less than the propeller commonly used of Thai fishermen. The new blade design had successfully reduced the severity of cavitation by stabilizing the tip vortex cavitation as evidenced from the preliminary study with CFD. However, this investigation suggests that the present approach is practicable as a design approach for low speed propeller for Thailands local fishery and related foundry industry only.

NOMENCLATURE

σ_n = Cavitation number based on n
$\sigma_n = (P_o - P_v)/(0.5\rho n^2 D^2)$

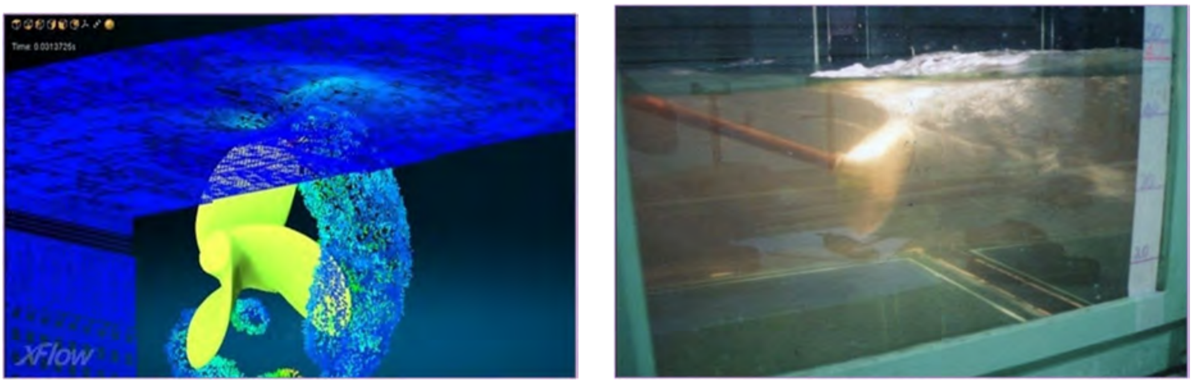

Figure 14: Illustration comparison between photo-experiment and X-Flow simulation at 750 rpm

Figure 15: Occurrence cavity at rotational speed 850 rpm. New-model; Type 3B-18-55

σ_v = Cavitation number based on V_s
$\sigma_n = (P_o - P_v)/(0.5\rho V_s^2)$

$C_P = (P - P_o)/(0.5\rho U_\infty^2)$ for otherwise
$C_P = (P - P_o)/(0.5\rho n^2 D^2)$ for propeller
$C_T = 2T/\rho A V_a$ for Thrust Coefficient,(A = Propulsion area)
$\eta_o = T \cdot V_a/2\pi NQ$, Propeller Efficiency
$\eta_t = T \cdot V_s/2\pi NQ$, Propulsive Efficiency
R_t = Total Ship resistance
J = Advance Coefficient, $J = V_a/ND$
J_s = Advance ratio based on V_s, $J_s = V_s/nD$
K_Q = Torque coefficient, $K_Q = Q/\rho n^2 D^5$
K_T = Thrust coefficient, $K_T = T/\rho n^2 D^4$
C_p = Pressure coefficient
D = overall diameter of the propeller
n = Propeller rotational frequency (rev/sec)
N = rotational speed of the propeller
p, q = Field point and variable point
P_o = Far upstream pressure, at the propeller Axis
P_{sat} = liquid saturated pressure, Pa
P_v = Vapor pressure of water
Q = Propeller torque
T = Propeller thrust
V_a = Inflow velocity
V_s = Ship speed

ACKNOWLEDGEMENTS

This study was partly supported by Nakon Si Thammarat Seaboard Industrial College, and I would like thank you Captain Saravut Wongngernyuang (RTN.), Royal Thai Navy for contributions toward this work.

REFERENCES

Andriotis, A. & Gavaises, M. (2008). 'Cavitation Formation and Development inside Transparent Diesel Injector Nozzle Replicas'. in Proc. ILASS-Europe, Como, Italy.

Carlton, J. (2012). Marine propellers and propulsion. Butterworth-Heinemann.

Dyson, C.W. (1924). Screw Propellers (T). Simmons-Boardman Publishing Co.Ltd. New York.

Francesco, S. & et al. (2003). 'A Viscous/Inviscous Coupled Formulation for Unsteady Sheet

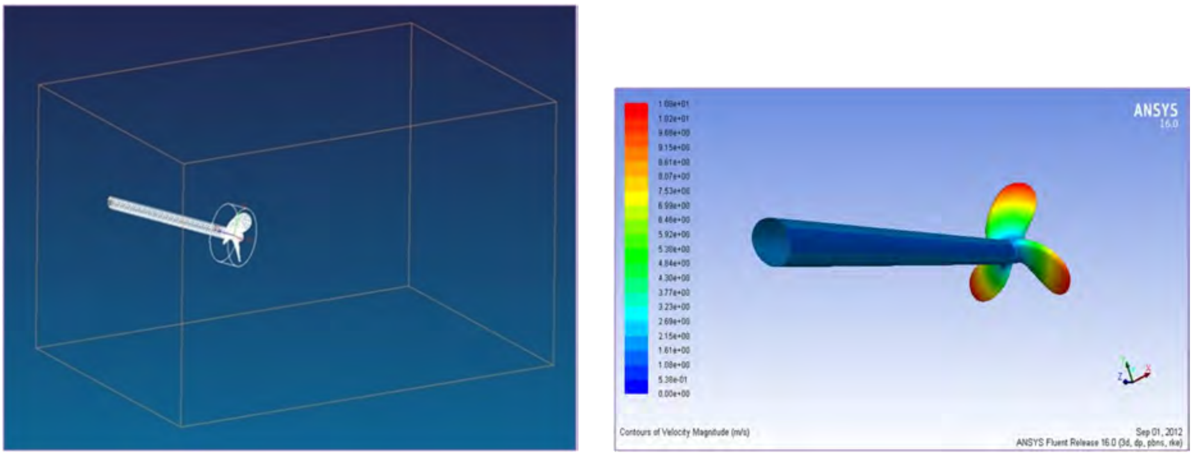

Figure 16: The computational domain of New-model propeller; Type 3B-18-55

Cavitation Modeling of Marine Propellers', 5th International Symposium on Cavitation. Osaka. Japan. 1-4 November.

Francisco, P. & et.al. (2002). 'Experimental and Numerical Investigation of the Cavitation Pattern on a Marine Propeller' 24th Symposium on Naval Hydrodynamics. Fukuoka. Japan. 8-13 July.

Greeley, D.S. & Kerwin, J.E. (1982). 'Numerical methods for propeller design and analysis in steady flow' SNAME Transaction **90**, pp. 415–453.

Hoeijmakers, H.W.M, Janaaens, M.E. & Kwan, W. (1998). 'Numerical Simulation of Sheet Cavitation [C]' 3rd International Symposium on Cavitation. Grenoble. France.

Jackson, D.H. (1920). Detail Design of Maine Screw Propellers (T). Pitman & Sons. London.

Kerwin, J., Kinnas, S. & Lee. (1987). 'Experimental and analytical techniques for the study of unsteady propeller sheet cavitation' 16th Symposium on Naval Hydrodynamics Berkeley. California.

Kerwin, J.E. (2001). Hydrofoils and Propellers Lecture Notes. Department of Ocean Engineering. Massachusetts Institute of Technology. USA. January.

Kerwin, J.E. (2003). 'The Preliminary Design of Advance Propulors' Proc. Of Propellers/Shafting Symposium SNAME. Virginia Beach. VA. USA. September 16-17.

Konno, A., Wakabayashi, K., Yamaguchi, H., Maeda, M., Ishii, N., Soejima, S. & Kimura, K. (2002). 'On the mechanism of the bursting phenomena of propeller tip vortex cavitation' Journal of Marine Science and Technology, **6**, pp. 181–192.

Kuiper, G. (2001). 'New developments around sheet and tip vortex cavitation on ships propellers' 4th International Symposium on Cavitation Pasadena.

Kutta, M. (1992). 'The Wageningen Propeller Series' Marin publication pp. 92-001.

Lerbs, H.W (2014). 'EFD and CFD Design and Analysis of a Propeller in Decelerating Duct' International Journal of Rotating Machinery Sep 16.

Lerbs, H.W. (1952). Moderately loaded propellers with a finite number of blades and an arbitrary distribution of circulation' SNAME Transaction **60**, pp. 73–117.

Rijsbergen, M.X. van & Kuiper, G. (1997) 'Modeling a cavitating vortex'. ASME Fluids Eng. Division Summer Meeting FEDSM97-3266. Vancouver.

Subhas, S., Saji, V.F., Ramakrishna, S. & Das, H.N. (2012) 'CFD Analysis of a Propeller Flow and Cavitation' International Journal of Computer Applications **55**, No.16, pp. 0975–8887.

Singhal, A.K., Athavale, M.M., Li, H. & Jiang, Y. (2002). 'Mathematical basis and validation of the full cavitation model' ASME Journal Fluids Engineering **124**, pp. 617–624.

O'Brien Cgia, T.P. & Amrina. (1969). The Design of Marine Screw Propellers (T). Huntchinson and Co.Ltd. London.

Vaz, G. & Bosschers, J. (2006). 'Modelling of three dimensional sheet cavitation on marine propellers using a boundary element method' 6th International symposium on cavitation. CAV2006. Wageningen. NL.

Wijngaarden, E. van, Bosschers, J. & Kuiper, G. (2005). 'Aspects of the cavitating propeller tip vortex as a source of inboard noise and vibration' FEDSM2005-77271, ASME Fluids Engineering Division Summer Meeting and Exhibition Houston. TX. USA.

Wijngaarden, E. van, Bosschers, J., Vaz, G. & Starke, A.R. (2008). 'Computation analysis of propeller sheet cavitation and propeller-ship interaction' RINA conference MARINE CFD 2008 Southampton. UK. March 26-27.

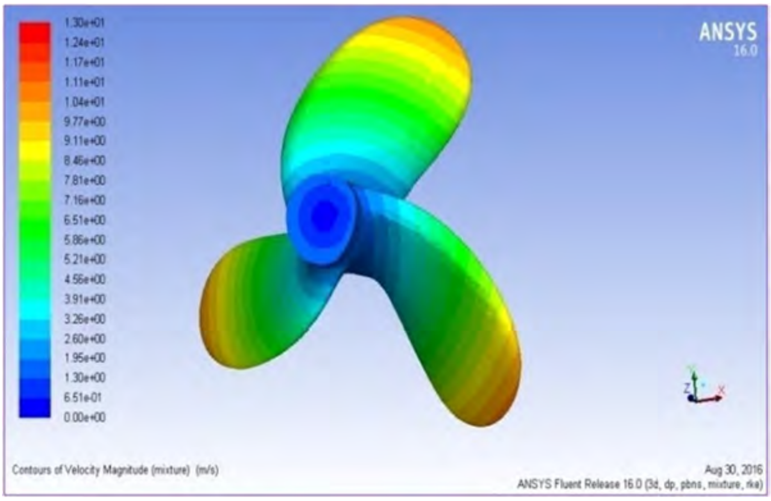

Figure 17: Contour plots of velocity at RPM 850, Js = 0.701 and $\sigma_n = 1.386$ of New-model; Type 3B-18-55

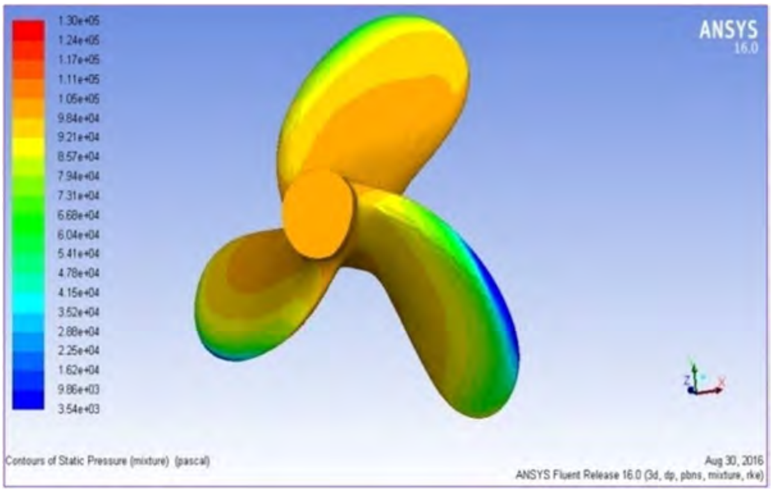

Figure 18: Contour plots of predicted static pressure patterns on suction (back) side at RPM 850, Js = 0.701 and $\sigma_n = 1.386$ of New-model; Type 3B-18-55

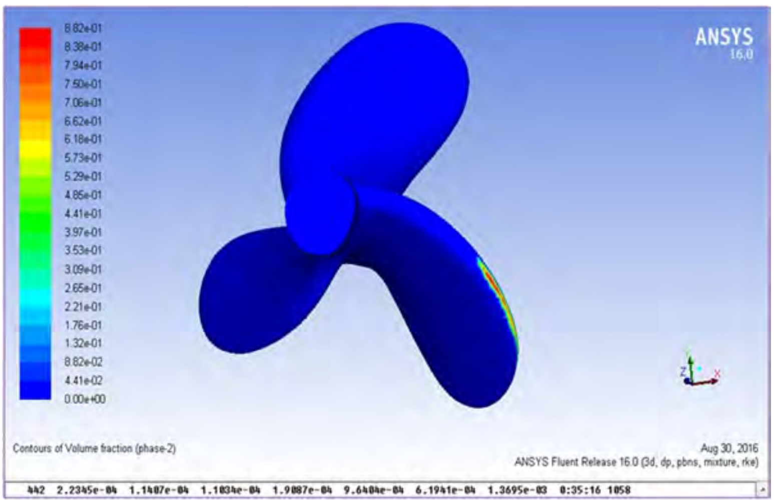

Figure 19: Contour plots of predicted volume fraction cavity patterns on suction (back) side at RPM 850, Js = 0.701 and $\sigma_n = 1.386$ of New-model; Type 3B-18-55